UC San Diego

UC San Diego Electronic Theses and Dissertations

Title

Flexible Thermoelectric Device for Localized Thermal Management

Permalink

https://escholarship.org/uc/item/9sc6d5bm

Author

Lee, Minjae

Publication Date

2016

Peer reviewed|Thesis/dissertation

eScholarship.org Powered by the California Digital Library
University of California

UNIVERSTIY OF CALIFORNIA, SAN DIEGO

Flexible Thermoelectric Device for Localized Thermal Management

A thesis submitted in partial satisfaction of the requirements
for the degree Master of Science

in

Master of Science in Materials Science and Engineering

by

Minjae Lee

Committee in charge:

Professor Renkun Chen, Chair
Professor Shengqiang Cai
Professor Yu Qiao

2016

Copyright

Minjae Lee, 2016

All rights reserved

The Thesis of Minjae Lee is approved, and it is acceptable in quality and form for publication on microfilm and electronically:

_____

_____

_____

Chair

University of California, San Diego

2016

Table of Contents

Signature iii
Table of Contents iv
List of Figures v
List of Tables vii
Acknowledgements viii
Vita ix
ABSTRACT OF THE THESIS x
Chapter 1 Introduction and Background 1
1.1 Motivation 1
1.2 Objectives and scope of the research 1
1.3 Working principle of thermoelectric devices 3
Reference 6
Chapter 2 Design and Fabrication of Thermoelectric Device 7
2.1 Process overview 7
2.2. Sparks-erosion of BST and BTS nanoparticles 8
2.3 Hot Pressing 10
2.4. Fabrication of Flexible TE Device 12
Reference 14
Chapter 3 Coefficient of Performance Measurements 15
3.1 Coefficient of Performance for TE Devices 15
3.2 COP Measurements on Flexible TE Devices 19
Reference 22
Chapter 4 Conclusion and Future Work 23

List of Figures

Figure 1.1. Schematic drawing of a TE device [4]. The device contains p- and n- type TE pillars that are connected in series electrically and in parallel thermally. 3
Figure 2.1. Schematic flow chart of the TE device fabrication process. 7
Figure 2.2. Schematic drawing of the spark erosion setup (left) and the spark erosion shaker pot (right) [1]. 8
Figure 2.3. The cell and dielectric liquid shaker-pot container (left) , and the cell, 10 cm in diameter, demonstrating the electrode links to the pulsed power source, and the perforate charge support (right) [2]. 9
Figure 2.4. Photographs of the spark erosion setup. (a) Two electrodes of the cell in the shaker-pot are joined to the electrodes of pulsed power, which is applied to the motor driven shaker. (b) The shaker-pot is immersed in the liquid nitrogen. 9
Figure 2.5. The schematic drawing of the hot pressing setup (adopted from Ref. [3]), and a photograph of a hot pressed pellet with 12.7 mm diameter and 4mm thickness. 11
Figure 2.6. Seebeck measurement results for p-type and n-type TE pillars. 11
Figure 2.7. Flexible TEC fabrication steps. (a-b) Array of p- and n-type BST pillars are located on a PDMS film, and between two PDMS followed by liquid PDMS. (c-d) Bi-Sn solder is pasted on each BST pillar site and annealed on Ag electrodes. (e-f) the opposite side interconnection by Ag is done in same manner of (c-d) 13
Figure 2.8. Photographs of flexible TEC fabrication process. (a) Flexibility of 70 um thick Ag electrode used for interconnection between TE pillars. (b) Array of 1 by 3 mm Ag electrodes assembled on PDMS film. (c) 4 by 4 arrays of TE pillars embedded PDMS with Bi-Sn solder. (d) After Ag electrodes connection. 13
Figure 3.1. Schematic of a TE device and its equivalent thermal resistance circuit model diagram showing the Joule heating, Peltier cooling/heating, and heat conduction effects. 16
Figure 3.2. (a) Schematic and (b) optical image of the COP measurement system where two additional TECs (i.e., TEC2 and TEC3) were controlled. 17
Figure 3.3. Controlled temperatures in response to the applied current to TEC2 and/or TEC3. Red arrows represent the time when the current was controlled. 17
Figure 3.4. (a) Measured temperatures at hot (red) and cold (blue) sides as a function of the current applied to commercial TEC for cooling while monitoring the heat flux. (b) Measured heat flux as a function of the current applied to commercial TEC for cooling. 18
Figure 3.5. (a) Measured temperatures at hot (red) and cold (blue) sides as a function of the current applied to commercial TEC for heating while monitoring the heat flux.

(b) Measured heat flux as a function of the current applied to commercial TEC for heating. 19
Figure 3.6. (a) Measured temperatures at hot (red) and cold (blue) sides as a function of the current applied to flexible TEC for cooling while monitoring the heat flux. (b) Measured heat flux as a function of the current applied to flexible TEC for cooling .. 20
Figure 3.7. Measured temperatures at hot (red) and cold (blue) sides as a function of the current applied to flexible TEC for heating while monitoring the heat flux. (b) Measured heat flux as a function of the current applied to flexible TEC for heating .. 21

List of Tables

Table 2.1: Summary of the results of TE property measurement..... 12
Table 3.1: Summary of the results of COP measuremnt with a commerial battery 21

Acknowledgements

First and foremost, I would like to express my sincere gratitude to my advisor for his support during my graduate year. I also want to thank my collaborators and coworkers at UC San Diego.

Vita

2015	Bachelor of Science, University of California, San Diego
2015-2016	Graduate Researcher Assistant, University of California, San Diego
2016	Master of Science, University of California, San Diego

ABSTRACT OF THE THESIS

Flexible Thermoelectric Device for Localized Thermal Management

by

Minjae Lee

Master of Science in Materials Science and Engineering

University of California, San Diego, 2016

Professor Renkun Chen, Chair

Flexible thermoelectric (TE) refrigerators are attractive for personalized thermal management, for example, when integrated into clothes. Flexible TE power generators can also find applications in wearable self-powered mobile electronics. These devices, however, need high thermoelectric performance and mechanical

flexibility under compressive and tensile strains, a combination of device properties that are often difficult to achieve. Despite significant efforts in the field, flexible TE devices, such as the ones made from organic materials, often exhibit lower cooling power than the actual needs. In this thesis, I studied flexible TE devices that offer high coefficient of performance.

In chapter 1, The motivation of personalized thermal management was provided. Fundamental aspects of thermoelectric devices were discussed.

In chapter 2, Technical approaches of making flexible TE devices were described. A flexible TE device was demonstrated.

In chapter 3, the coefficient of performance (COP) measurement results were presented and discussed. Specifically, COP for cooling and heating applications was measured.

In chapter 4, conclusions drawn from this study were summarized. Future work was suggested.

Chapter 1

Introduction and Background

1.1 Motivation

Approximately 13% of all primary energy consumed in the United States is attributed to the heating, ventilating, and air conditioning (HVAC) of buildings [1], accounting for around 13% of greenhouse gas emission. For cooling purposes, around 4 QBtu of energy is consumed. If the energy consumption in HVAC can be reduced by 15%, this would not only reduce primary energy consumption, but would also reduce the emission of greenhouse gases.

1.2 Objectives and scope of the research

One of the attractive approaches to reduce HVAC energy consumption is to expand the temperature set point span of buildings. For the purpose of expanding a building's neutral temperature set point window from 70-75 ℉ to 66-79 ℉, or extending by 4 ℉ in both directions, it is necessary to place localized thermal envelopes around individuals as a means of managing the thermal balance in order to maintaining thermal comfort. Analysis reveals that a 20% change in the thermal resistance of clothing could lead to approximately 4 ℉ temperature change, if the metabolic rate of an individual is 58 W/cm^2. For the purpose of enabling a simple scaling, the steady state heat flux through a planar wall (i.e., the cloth) is shown as:

$$q'' = \left(\frac{1}{R}\right) \cdot (T_0 - T_1) \qquad \text{Eq 1.1}$$

In Eq.1.1, T_1 represents the ambient temperature, T_0 represents the skin temperature, and *R* represents the overall thermal resistance. If we assume that the thermal resistance is fixed while T_1 changes to T_2, then the difference in the heat flux would be: .

$$\Delta q'' = \left(\frac{1}{R}\right) \cdot (T_2 - T_1) \qquad \text{Eq 1.2}$$

With the result that heat flux percentage change is:

$$\frac{\Delta q''}{q''} = \frac{(T_2 - T_1)}{(T_0 - T_1)} \qquad \text{Eq 1.3}$$

The comfortable skin temperature (T_0) is around 93°F. When T_1 = 75°F and T_2 = 79°F, $\Delta q''/q''$ is 22.2% according to Eq. 1.3. Likewise, when the ambient temperature decreases from T_1 =70°F to T_2 = 66°F, $\Delta q''/q''$ is -17.3% to maintain the same comfortable skin temperature (namely, 93°F). When an adult is immobile, with a base metabolic rate of 58.2 W/m^2 and an average body surface area of 1.8 m^2, the total metabolic power is q'' =105 W [2]. In other word, once the ambient temperature increases from 75 to 79°F, in order to maintain the same skin temperature, 23 W or 22% of metabolic power must be removed. If the ambient temperature is decreased from 70 to 66°F, in order to keep the same skin temperature, it is necessary to supply 18 W, or 17% of metabolic power.

The skin temperature can also be maintained by modifying the thermal resistance of the clothing when the ambient temperature changes. In order to change

the ambient temperature from T_1 to T_2 while maintaining the same heat flux and skin temperature, the thermal resistance should be changed from R_1 to R_2:

$$\frac{R_2}{R_1} = \frac{T_0 - T_1}{T_0 - T_2} \qquad \text{Eq 1.4}$$

1.3 Working principle of thermoelectric devices

A TE device is typically comprised of two ceramic layers shrouding semiconductor TE pillars (See Figure1.1). The ceramic top and bottom surfaces are necessary for maintaining the stability of the device and for its low electrical conductivity and high thermal conductivity. As such, the significance of the ceramic plates lies in their ability to insulate electricity within the semiconductor layer and its ability to facilitate the transfer of maximum heat from one side of the ceramic to the other side.

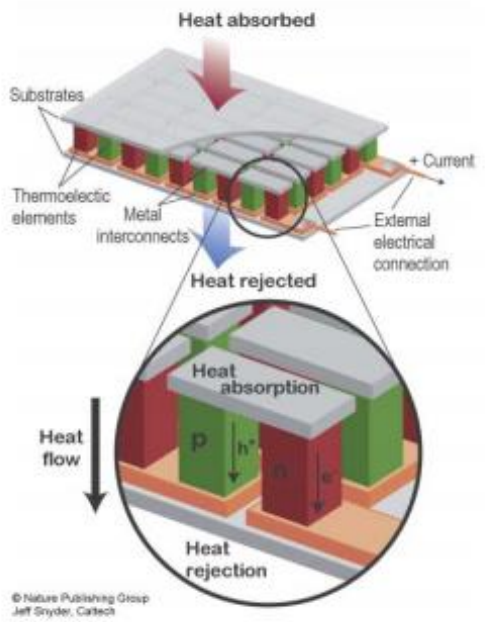


Figure 1.1. Schematic drawing of a TE device [3]. The device contains p- and n- type TE pillars that are connected in series electrically and in parallel thermally.

Bismuth telluride (Bi_2Te_3) and its alloys are most commonly utilized for creating state-of-the-art TE devices because of their relative high efficiency at around room temperature [4]. For wearable personalized thermal management applications, in which the temperature gradient is on the order of 2-4 ^oC around room temperature, Bi_2Te_3 based alloy are suitable, for the requirement of high efficiency at small temperature gradient. Other common TE materials are Lead Telluride (PbTe) and SiGe for higher temperature applications [5, 6]. In this study, we focused on Bi_2Te_3 based modules for room temperature applications.

Thermoelectric properties of materials are commonly quantified by the Seebeck and Peltier coefficients (*S* and Π). The efficiency of a TE device is related to its TE figure of merit ZT,

$$ZT = \left(\frac{S^2\sigma}{\kappa}\right)T \qquad \text{Eq. 1.5}$$

In the above equation, Seebeck coefficient is denoted as S, electrical conductivity is denoted as σ, thermal conductivity is denoted as κ and temperature is denoted as T. Thermoelectric power is defined as $S^2\sigma$.

Electronic thermal conductivity κ_e plus the lattice thermal conductivity κ_l contribute to the thermal conductivity in the equation ($\kappa = \kappa_e + \kappa_l$). In metals, a long contribution of the thermal conductivity κ comes from the electronic thermal conductivity κ_e. In semiconductors, thermal conductivity is primarily contributed by lattice thermal conductivity κ_l.

In accordance to the Wiedeman Franz Law, thermal conductivity increases when the electrical conductivity increases:

$$\kappa = \left(\frac{3k_B{}^2}{2e^2}\right)\sigma T \qquad \text{Eq. 1.6}$$

$$\kappa = L\sigma T \qquad \text{Eq. 1.7}$$

In the above equations, the total thermal conductivity is denoted as κ, Boltzmann constant is denoted as k_B, electron charge is denoted as e , electrical conductivity is denoted as σ, Lorenz number is denoted as L, and temperature is denoted as T. The Lorentz number is derived from fundamental constants and is $2.44\times10^{-8}\ W\Omega/K^2$, which could deviate slightly in certain materials, such as TE materials.

Reference

1. Buildings Technologies Program, Energy Efficiency and Renewable Energy, U.S. Department of Energy: 2011 Buildings Energy Data Book, March 2012.

2. Bradshaw, V. The Building Environment: Active and Passive Control Systems, 3rd Edition, Wiley Publishing, May 200

3. G. Jeffrey Snyder and Eric S. Toberer. "Complex thermoelectric materials." Nature Materials 7, 105 - 114 (2008). doi:10.1038/nmat2090

4. Rowe, D.M. CRC Handbook of Thermoelectrics. (1st ed.) Boca Raton, FL : CRC Press.

5. Z.H. Dughaish. "Lead telluride as a thermoelectric material for thermoelectric power generation". Physica B: Condensed Matter. Volume 322, Issues 12, September 2002, Pages 205223.

6. Ranita Basu. "Improved thermoelectric performance of hot pressed nanostructured n-type SiGe bulk alloys". J Mater. Chem. A, 2014 , 2, 6922-6930

Chapter 2

Design and Fabrication of Thermoelectric Device

2.1 Process overview

Figure 2.1 shows an overview of the fabrication process. The process started with bulk materials of BST ($Bi_{0.5}Sb_{1.5}Te_3$) and BTS ($Bi_2Te_{2.8}Se_{0.2}$), and from the bulk materials the fine powders were produced by the spark-erosion process. Then under condition of high temperature and pressure, round solid samples were produced. The cut 1x1 mm^2 pillars were then fully embedded into a polydimethysiloxane (PDMS) matrix, with terminal of both sides of pillars exposed so that electrical electrodes could be made. Finally flexible silver films are applied on the pillars for electrical connection.

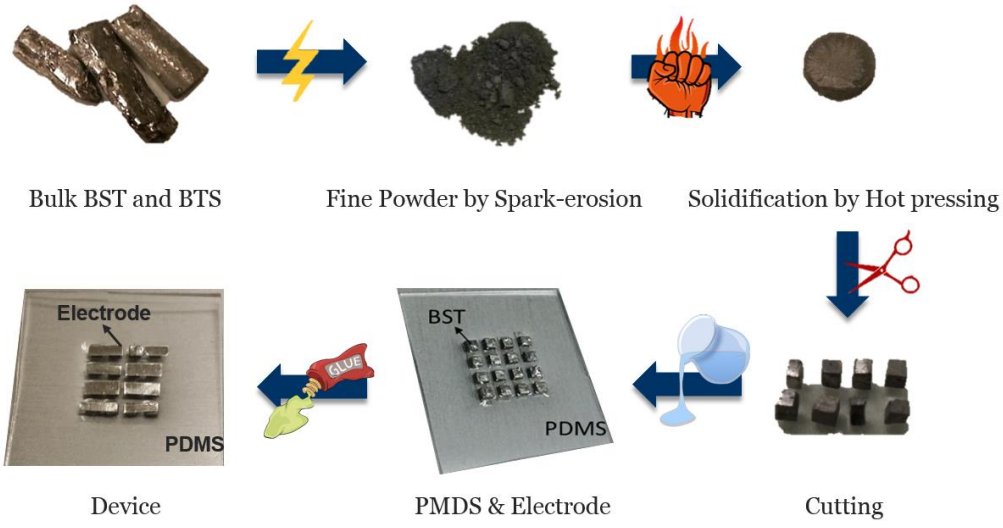


Figure 2.1. Schematic flow chart of the TE device fabrication process.

2.2. Sparks-erosion of BST and BTS nanoparticles

Fine BST and BTS powders were produced via spark-erosion. These fine powders were produced through spark erosion when a charged capacitor was attached to electrodes bearing chargers/starting material that are the same as those of the charged capacitor (Figure 2.2).

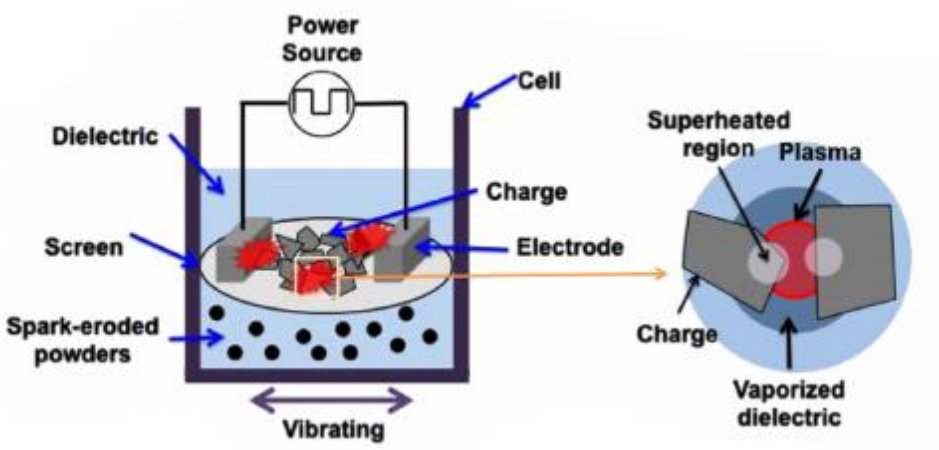


Figure 2.2. Schematic drawing of the spark erosion setup (left) and the spark erosion shaker pot (right) [1].

A spark is generated through the application of a electric field larger than the dielectric breakdown field. All of the system, including the electrodes and chargers, function in a dielectric liquid (in this instance, liquid nitrogen was utilized) to safeguard against oxidation of BST as exhibited in Figure 2.3.

The procedure is a repetition of spark emissions among chunks as demonstrated in Figure 2.4, which leads to excessively high temperatures (10,000 K)[2]. The spark emissions cause molten droplets or vaporized material which freezes in the liquid nitrogen, producing fine particles.

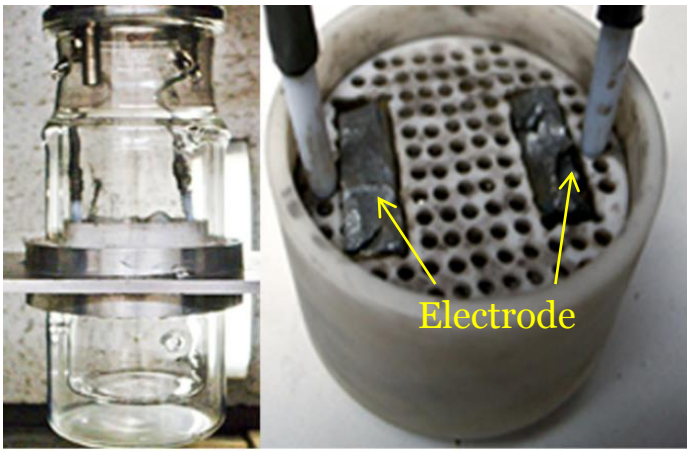


Figure 2.3. The cell and dielectric liquid shaker-pot container **(l**eft) and the cell, 10 cm in diameter, demonstrating the electrode links to the pulsed power source, and the perforate charge support (right) [2].

In addition, a "shaker-pot" was used through the use of a motor for enhancing the rate of production. A spark erosion cell in diameter is glass container containing the dielectric liquid (liquid nitrogen).

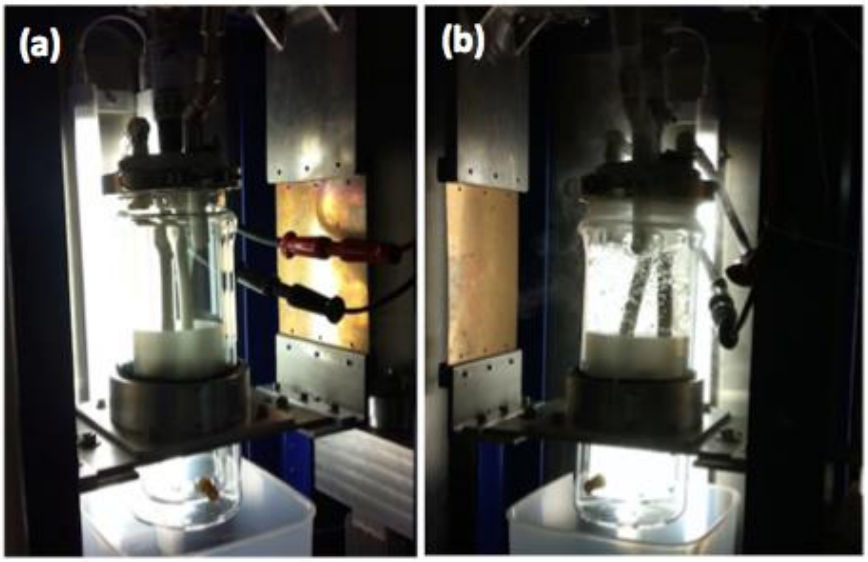


Figure 2.4 Photographs of the spark erosion setup. (a) Two electrodes of the cell in the shaker-pot are joined to the electrodes of pulsed power, which is applied to the motor driven shaker. (b) The shaker-pot is immersed in the liquid nitrogen.

The small particles were produced by quenching molten droplets or vaporized materials. The spark-eroded particles have a wide size distribution, ranging from nm to μm. After they were sieved with 45 μm mesh, this size distribution, while not ideal, is suitable for our preliminary work for making TE devices. Further refinement of the TE particles could lead to better result and may warrant further study.

2.3 Hot Pressing

The spark-eroded particles were consolidated into solid pellets by using a home-made hot pressing system, as shown in Fig. 2.5. The materials used in our study were p-type bismuth antinomy telluride ($Bi_{0.5}Sb_{1.5}Te_3$) and n-type bismuth telluride selenite ($Bi_2Te_{2.8}Se_{0.2}$). Spark-eroded powders were hot pressed under a range of selected conditions of pressure, time and temperature; 90MPa, 5 minutes, and 450℃. Hot pressing was performed under vacuum using a hot pressing equipment (Figure 2.5) based on a vacuum chamber and an induction heating furnace.

With the consolidated pellets, we measured Seebeck coefficient and electrical conductivity, and estimated the ZT value by assuming a constant thermal conductivity of 1.5 W/m-K. The result of the Seebeck coefficient of n-type and p-type is shown in Figure 2.6. X-axis and Y-axis represent temperature difference and voltage respectively, and from the slope of the measured data, Seebeck coefficients were obtained. The electrical conductivities were measured by using the four-point probe method. The thermal conductivity was not measured due to the difficulty of measuring in-plane thermal conductivity, but rather it was assumed at 1.5 W / m·K. Actual thermal conductivity of the hot-pressed pellets would most likely be lower due to the

presence of the nanoscale and microscale grains in the samples. The ZT values were estimated. The resulted were summarized in Table 2.1.

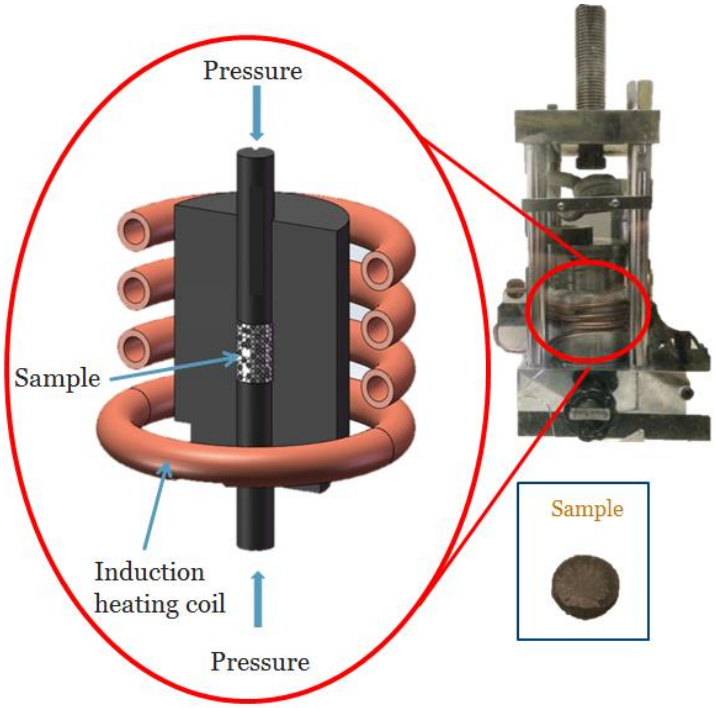


Figure 2.5. The schematic drawing of the hot pressing setup (adopted from Ref. [3]), and a photograph of a hot pressed pellet with 12.7 mm diameter and 4mm thickness.

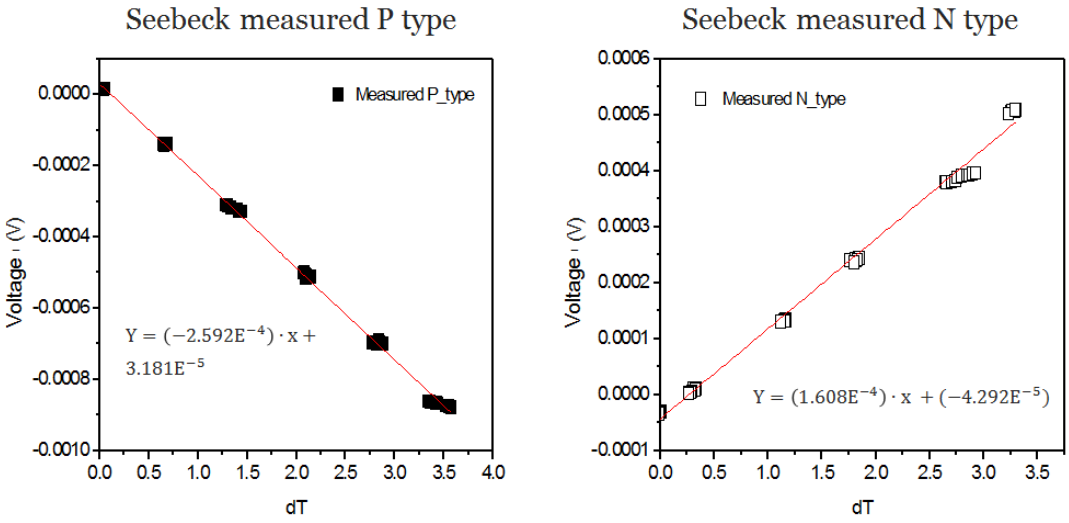


Figure 2.6. Seebeck measurement results for p-type and n-type TE pillars.

Table 2.1. Summary of the results of TE property measurements

Seebeck Coefficient	Electrical Conductivity	Thermal Conductivity (assumed, not measured)	ZT
$S_p = 259.2\ \mu V/K$	$\sigma_p = 707.22\ S \cdot cm^{-1}$	1.5 W/m·K	$ZT_p = 0.933$
$S_n = -160.8\ \mu V/K$	$\sigma_n = 1283.5\ S \cdot cm^{-1}$		$ZT_n = 0.657$

2.4. Fabrication of Flexible TE Device

We have developed an approach for flexible TEC fabrication from assembly of components by series of stamping transfers. The detail process is illustrated in Fig. 2.7. To begin with, both p- and n-type TE pillars of 1.4 mm square size were aligned on a flat PDMS substrate with 1 mm spacing. After alignment and positioning of the TE pillars, they were covered by another PDMS plate followed by filling and curing of liquid PDMS to fully embed the TE pillars. After curing, the top and bottom plates were removed, resulting in TE-PDMS plate with both top and bottom TE terminals exposed. For electrical connection between TE pillars, ~70 um thick Ag film is diced into 1 by 4 mm size and positioned in an array as shown in Fig. 2.8(b). Also, one side of surface of TE pillars are coated with Bi-Sn soldering paste to ensure low contact resistance between the Ag electrodes and the TE pillars. Fig. 2.8(c) shows the result of TE pillars embedded in PDMS substrate with Bi-Sn solder coated on each TE pillars. Connecting TE pillars through Ag electrodes is done by overlaying array of Ag electrodes on top of TE-PDMS and annealing at 170 ^{o}C for 1 min. Electrical connection at the opposite surface is also done by same manner depicted in Fig. 2.7(e) and Fig. 2.8(d). The active TE device area is 1x1 cm^2.

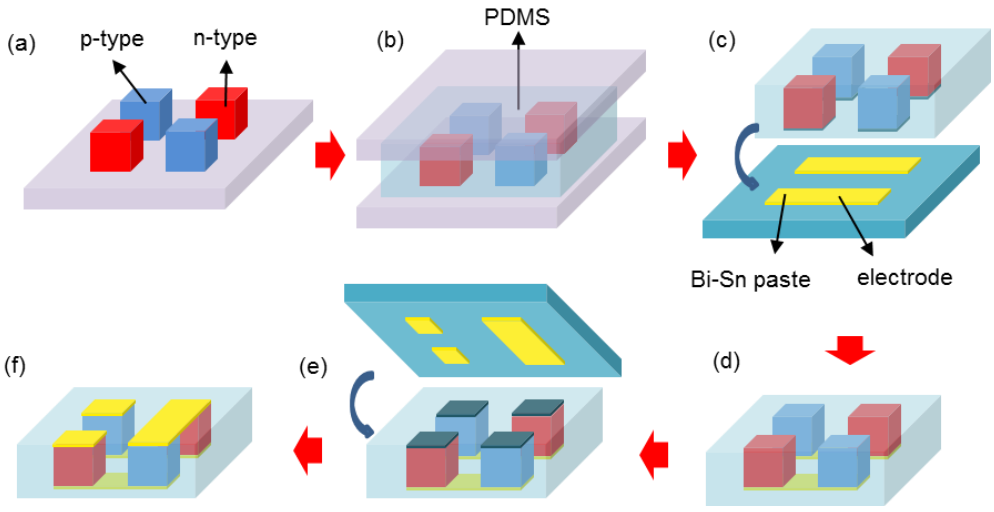


Figure 2.7. Flexible TEC fabrication steps. (a-b) Array of p- and n-type BST pillars are located on a PDMS film, and between two PDMS followed by liquid PDMS. (c-d) Bi-Sn solder is pasted on each BST pillar site and annealed on Ag electrodes. (e-f) the opposite side interconnection by Ag is done in same manner of (c-d)

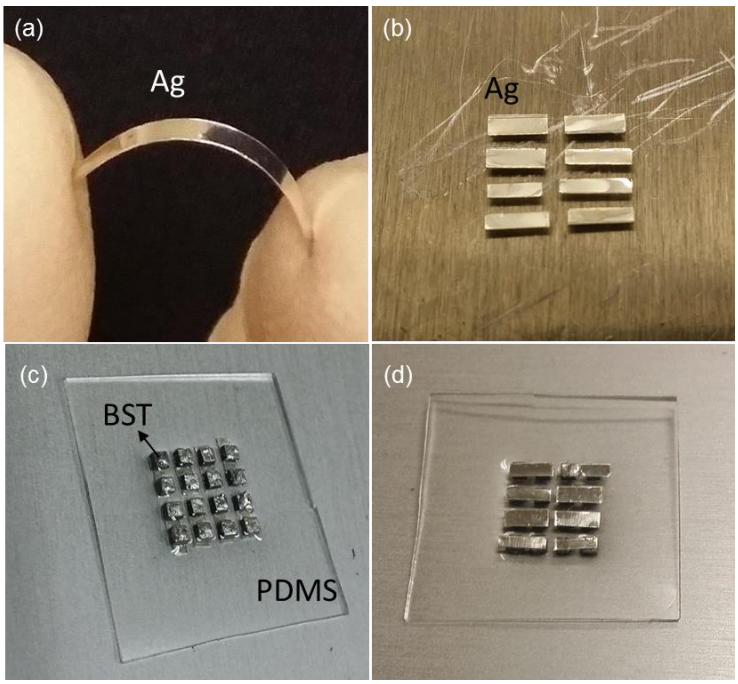


Figure 2.8. Photographs of flexible TEC fabrication process. (a) Flexibility of 70 um thick Ag electrode used for interconnection between TE pillars. (b) Array of 1 by 3 mm Ag electrodes assembled on PDMS film. (c) 4 by 4 arrays of TE pillars embedded PDMS with Bi-Sn solder. (d) After Ag electrodes connection.

Reference

1. J Moon et al., “High performance multi-scaled nanostructured spectrally selective coating for concentrating solar power”, Nano Energy 8, 238-246 (2014)

2. P K Nguyen et al., "Spark erosion: a high production rate method for producing $Bi_{0.5}Sb_{1.5}Te_3$ nanoparticles with enhanced thermoelectric performance”, Nanotech 23 415604 (7pp) (2012)

3. Henriques, B et al., “Effect of Hot Pressing Variables on the Microstuructrue, Relative Density and Hardness of Sterling Silver (Ag-Cu alloy) Powder Compacts” Materials Research.17(3):664-671 (2014)

Chapter 3

Coefficient of Performance Measurements

3.1 Coefficient of Performance for TE Devices

The coefficient of performance (COP) is used to measure the refrigeration efficiency of a refrigerator, or the heating efficiency of a heat pump. The COP is defined as the cooling or heating thermal power produced by the refrigerator or the heat pump respectively, divided by the electrical power consumed by the same unit. The COP of the TE devices can be written as:

$$\mathrm{COP} = \frac{\mathrm{N}\left[\ \mathrm{S}\cdot\mathrm{I}\cdot\mathrm{T_c} - \frac{1}{2}\mathrm{I}^2\mathrm{R_{TE}} - \mathrm{G_{TE}}(\mathrm{T_H}-\mathrm{T_C})\ \right]}{\mathrm{N}\left[\mathrm{I}^2\mathrm{R_{TE}} + \mathrm{S}\cdot\mathrm{I}(\mathrm{T_H}-\mathrm{T_C})\right]} \qquad \text{Eq 3.1}$$

Where $\mathrm{I}^2\mathrm{R_{TE}}$ indicates a Joule heating, $\mathrm{G_{TE}}(\mathrm{T_H}-\mathrm{T_C})$ is a heat flux of the thermal conduction of TE, S is the Seebeck coefficient, and $\mathrm{R_{TE}}$ is a thermal resistance of TE.

A TE device as well as the equivalent thermal resistance circuit model diagram is shown in Figure 3.1. The balance of heat between Q_C and Q_H can be used for analyzing TE model having power input. Making use of a TE system to cool should be larger than Joule heating and the conduction of heat via TE pillars [1]. Whenever there is a current, the absorbed heat is at the top of the TE pillars, and released at the base of TE pillars.

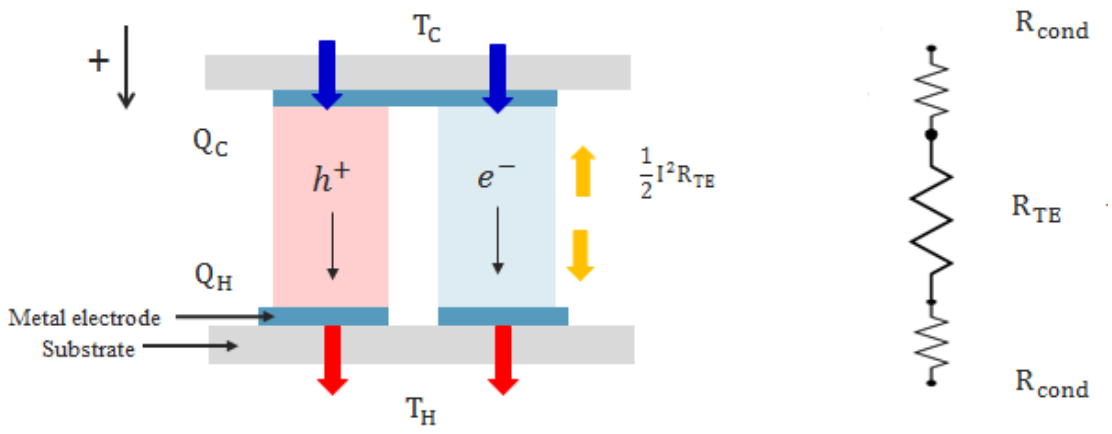


Figure 3.1. Schematic of a TE device and its equivalent thermal resistance circuit model diagram showing the Joule heating, Peltier cooling/heating, and heat conduction effects.

3.2. COP Measurement Setup with Commercial TE Modules

COP was measured under the boundary conditions of fixed temperatures at cold and hot sides. The boundary conditions for constant temperatures were realized by attaching two additional TECs at the top and bottom of the TEC to be measured as shown in Fig. 3.2. The temperatures were monitored while measuring the heat flux at the skin-side and the targeted temperatures were achieved by applying the power into the TEC2 and TEC3 as shown in in Fig. 3.2, such as 79 ^{o}F and 75 ^{o}F at hot and cold sides, respectively, for cooling, and 70 ^{o}F and 66 ^{o}F at hot and cold sides, respectively, for heating.

Fig. 3.3 showed controlled temperatures while operating the TEC for cooling. To achieve the targeted temperatures power was applied into TEC2 and TEC3 as is indicated on Fig 3.3.

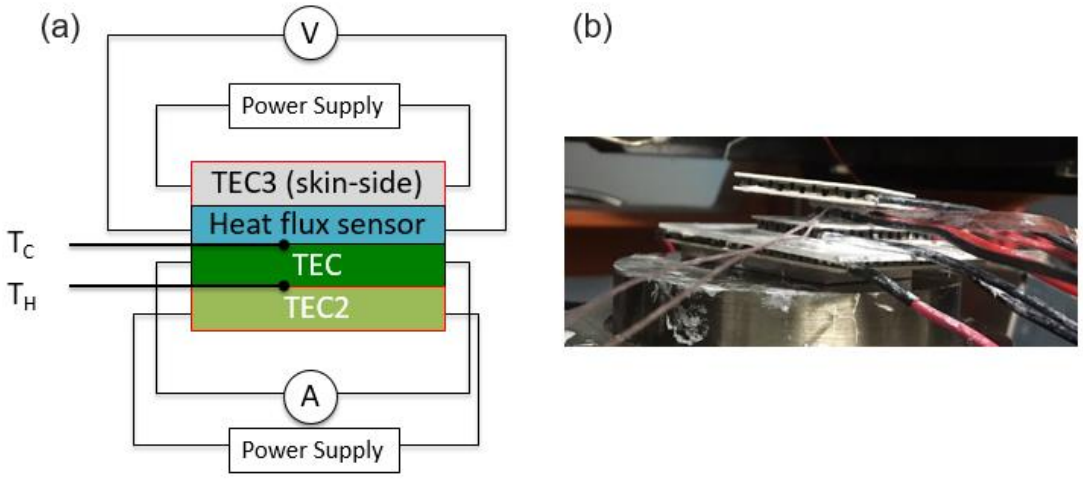


Figure 3.2. (a) Schematic and (b) optical image of the COP measurement system where two additional TECs (i.e., TEC2 and TEC3) were controlled.

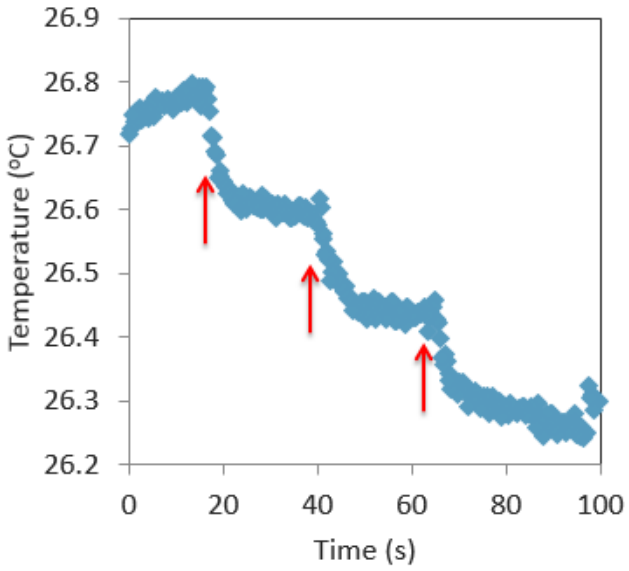


Figure 3.3. Controlled temperatures in response to the applied current to TEC2 and/or TEC3. Red arrows represent the time when the current was controlled.

Here we used a commercial TEC (00711-5L31-12CB, Custom Thermoelectric) to setup the COP measurement system. Average temperature of 78.99 ^{o}F and 75.24 ^{o}F was achieved with the standard deviation of 0.045 ^{o}F and 0.077 ^{o}F for hot and cold sides, respectively. The temperatures were effectively controlled in that the average

values were very close to the targeted temperatures of 79 ^{o}F and 75 ^{o}F, and the standard deviations were negligibly small. Under the measurement conditions, heat flux was measured using a heat flux sensor.

Fig. 3.4 showed heat flux at the operating current of TEC. Low current input to the TEC resulted in the negative heat flux where heat flows from the air to the "skin" (or from the hot side to the cold side) due to the heat conduction from the air-side (79 ^{o}F) to the "skin"-side (75 ^{o}F). As increasing the operating current, cooling effect by TEC increased and the cooling heat flux of 5.8 mW/cm^2 could be achieved at the current of 209.5 mA, due to the TE Peltier effect. The heat flux of 5.8 mW/cm^2 implies the net cooling effect of 1.3 mW/cm^2 from the TEC under the fixed temperature conditions. Therefore, we could get the COP of 0.38 for cooling. Here COP cooling was defined as

$$\mathrm{COP}_{\mathrm{cooling}} = \frac{1.3\ \mathrm{mW}}{\mathrm{I}^2\mathrm{R}} \qquad \text{Eq 3.2}$$

where $\mathrm{I} = 209.5$ mA and R is the internal resistance of the TEC (=0.078 Ω).

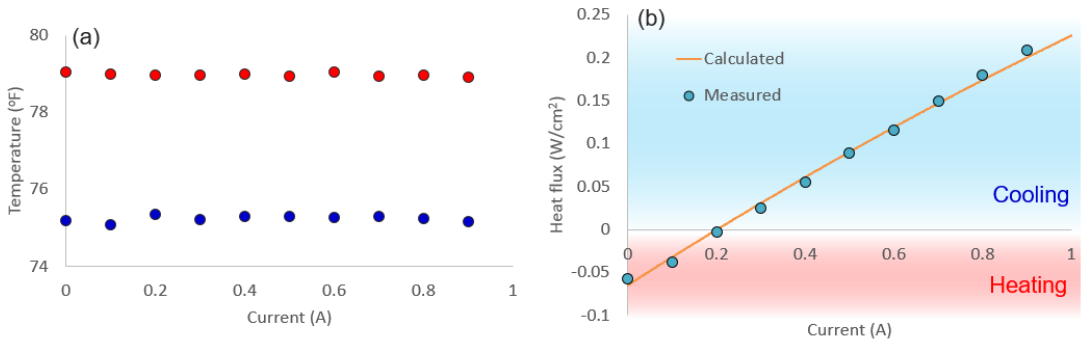


Figure 3.4. (a) Measured temperatures at hot (red) and cold (blue) sides as a function of the current applied to commercial TEC for cooling while monitoring the heat flux. (b) Measured heat flux as a function of the current applied to commercial TEC for cooling.

Similarly, COP for heating was measured with different temperature conditions, 70 ^{o}F at hot side and 66 ^{o}F at cold side. As shown in Fig. 3.5, due to the higher temperature at the skin-side, the heat flows from the skin to the air (cooling) at low current. 201 mA current lead to the heat flux of 5.8 mW/cm^2, implying the 1 mW/cm^2 for heating power. The COP for heating was obtained by using Eq 3.3

$$\mathrm{COP}_{\mathrm{heating}} = \frac{1.0\ \mathrm{mW}}{\mathrm{I}^2\mathrm{R}} \qquad \text{Eq 3.3}$$

where I = 201 mA and R is the internal resistance of the TEC (=0.078 Ω).

As a result, the COP of 0.32 was achieved with the controlled constant temperatures, where the average temperature was 69.90 ^{o}F and 65.99 ^{o}F, and the standard deviation was 0.269 ^{o}F and 0.196 ^{o}F for hot and cold sides, respectively.

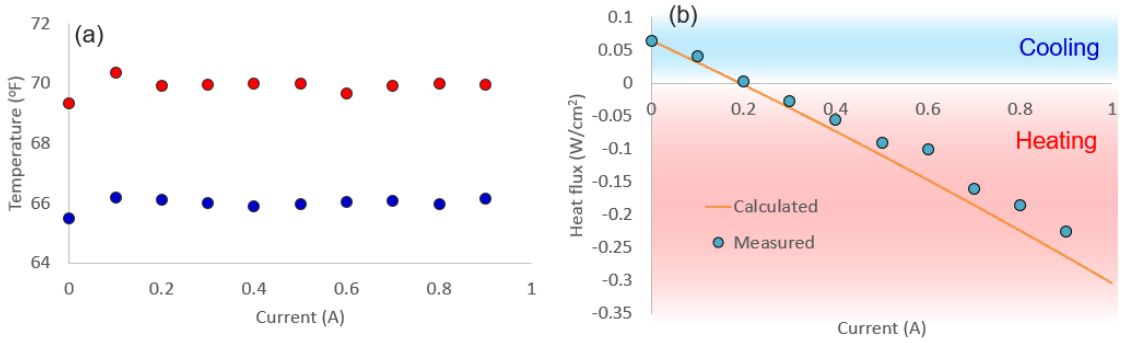


Figure 3.5. (a) Measured temperatures at hot (red) and cold (blue) sides as a function of the current applied to commercial TEC for heating while monitoring the heat flux. (b) Measured heat flux as a function of the current applied to commercial TEC for heating.

3.3 COP Measurements on Flexible TE Devices

Based on the measurement setup with the commercial TE devices shown in the previous section, COP was measured with the flexible TE device with the flexible

matrix (PDMS). Firstly, to evaluate the cooling effect, temperature conditions were controlled to be constant at 79°F and 75°F at hot and cold sides, where the average temperatures were 79.01°F and 75.23°F and the standard deviations were 0.016°F and 0.061°F. Using the Eq 3.2, COP of 0.24 was obtained at the operating current I = 261 mA, where the internal resistance of the TEC was measured as 0.08 Ω (Fig. 3.6). Similarly, COP of the flexible TE device for heating was measured under the boundary conditions, i.e., 70°F at hot side and 66°F at cold side. With the Eq 3.3, COP of 0.35 was achieved when I = 190 mA (Fig. 3.7). Also, a commercial battery was used to apply the current to the flexible TE device, where the external resistance was controlled to input suitable current to achieve total heat flux around 5.8 mW/cm^2. The results with a commercial battery were summarized in Table 3.1.

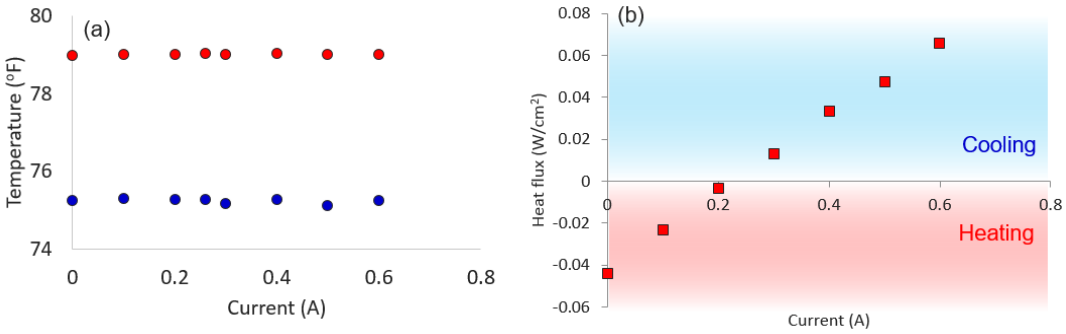


Figure 3.6. (a) Measured temperatures at hot (red) and cold (blue) sides as a function of the current applied to flexible TEC for cooling while monitoring the heat flux. (b) Measured heat flux as a function of the current applied to flexible TEC for cooling

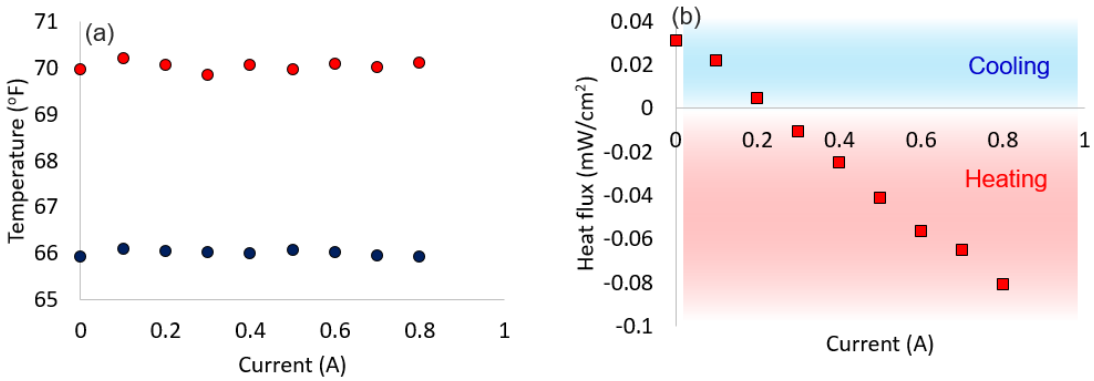


Figure 3.7. Measured temperatures at hot (red) and cold (blue) sides as a function of the current applied to flexible TEC for heating while monitoring the heat flux. (b) Measured heat flux as a function of the current applied to flexible TEC for heating

Table 3.1: Summary of the results of COP measurement with the commercial battery.

Cooling	External R (Ω)	Current (A)	T_{skin} (°C)	T_{air} (°C)	Measured voltage (V)	Heat flux (W/m^2)	Heat flux (mW/cm^2)
	10	0.278	26.093	23.912	7.54E-04	5.16E+01	5.16E+00
	I(@5.16 mW/cm^2) = 0.278 A → I(@5.8 mW/cm^2) = 0.282 A, **COP**=(1.3mW))/(282mA)^2(0.080)=**0.204**						
Heating	External R (Ω)	Current (A)	T_{skin} (°C)	T_{air} (°C)	Measured voltage (V)	Heat flux (W/m^2)	Heat flux (mW/cm^2)
	10	0.217	18.916	21.098	-6.51E-04	-4.46E+01	-4.46E+00
	I(@-1.69 mW/cm^2) = 0.217 A → I(@5.8 mW/cm^2) = 0.194 A, **COP**=(1.0mW))/(194mA)^2(0.080)=**0.332**						

Reference

1. M Antonik, B O'connor, S Ferguson "Performancce and Design comparison of a Bulk Thermoelectric Cooler With a Hybrid Architecture" Vol. 8 / 021022-1 (2016)

Chapter 4

Conclusion and Future Work

Flexible and high performance TE devices are highly attractive for localized thermal management systems to reduce energy consumption in building HVAC systems. In this thesis, PDMS based flexible TE devices were developed with a flexible electrode transfer technique. The coefficient of performance of the flexible thermoelectric devices was measured to be 0.24 in cooling and 0.355 in heating. The other advantage of this method is that scale-up of the flexible TE generator might be readily achieved because of the simplicity of the process of development. It may be anticipated that this technique can unravel more large-scaled flexible TE applications as well as hybrid energy harvesting systems coupled with vehicle components and solar cells.